Journal of Power Sources 186 (2009) 1–9

Contents lists available at ScienceDirect

Journal of Power Sources

journal homepage: www.elsevier.com/locate/jpowsour

Surface modification of carbon fuels for direct carbon fuel cells

Xiang Li[a], Zhonghua Zhu[a,*], Jiuling Chen[a], Roland De Marco[b], Andrew Dicks[a], John Bradley[a], Gaoqing Lu[a]

[a] Division of Chemical Engineering, School of Engineering, University of Queensland, Brisbane 4072, Australia
[b] Department of Applied Chemistry, Curtin University Technology, Perth, Australia

ARTICLE INFO

Article history:
Received 5 June 2008
Received in revised form
10 September 2008
Accepted 11 September 2008
Available online 27 September 2008

Keywords:
Carbon
Direct carbon fuel cell
Surface treatment
Electrochemical reactivity
Pre-treatment
Oxygen functional groups

ABSTRACT

The direct carbon fuel cell (DCFC) is a promising power-generation device that has much higher efficiency (80%) and less emissions than conventional coal-fired power plants. Two commercial carbons (activated carbon and carbon black) pre-treated with HNO_3, HCl or air plasma are tested in a DCFC. The correlation between the surface properties and electrochemical performance of the carbon fuels is explored. The HNO_3-treated carbon fuels have the highest electrochemical reactivity in the DCFC due to the largest degree of surface oxygen functional groups. The overall effect on changing the electrochemical reactivity of carbon fuels is in the order HNO_3 > air plasma ≈ HCl. Product gas analysis indicates that complete oxidation of carbon to CO_2 can be achieved at 600–700 °C.

1. Introduction

The direct carbon fuel cell (DCFC), the only fuel cell capable of converting solid carbon into electricity without a reformation process, is gaining increasing attention due to its high conversion efficiency with low pollution. Solid carbon fuels used in the DCFC can be produced easily from various sources that include coal, petroleum, natural gas and even biomass. Compared with other hydrogen-based fuel cells, the DCFC has the significant thermodynamic advantage of a near-zero entropy change at high temperature, i.e., the theoretical electrochemical efficiency of the DCFC ($\Delta G/\Delta H$) is almost 100% [1–7]. Even under practical conditions, about 80% efficiency can be reached in the DCFC system. The activities (chemical potentials) of both reactant carbon and the product carbon dioxide are fixed, and this results in a stable carbon anode potential during practical cell operation [2,3]. Finally, the DCFC has lower emissions compared with conventional power plants. In principle, the off-gas can be pure carbon dioxide, which can be directly collected for industrial use [1] or committed to storage.

Various electrolytes such as molten carbonates [2,3,8–13], molten hydroxides [7,14–17] and yttria-stabilised zirconia (YSZ)-based solid electrolytes [18,19] have been used in DCFCs. The latest development in DCFC technology is to utilize highly reactive carbon particulates dispersed in a molten carbonate electrolyte, which flows between the anode and cathode at high temperature [2,3,9,11,12]. The anode and cathode reactions may be expressed by Eqs. (1) and (2), respectively. The overall reaction and anode potential are given by Eqs. (3) and (4), respectively [2,12].

$$\text{Anodereaction}: C + 2CO_3^{2-} \rightarrow 3CO_2 + 4e^- \quad (1)$$

$$\text{Cathodereaction}: O_2 + 2CO_2 + 4e^- \rightarrow 2CO_3^{2-} \quad (2)$$

$$\text{Overallreaction}: C + O_2 \rightarrow CO_2 \quad (3)$$

where the anode potential is given by

$$E_{\text{anode}} = E^{\circ} - (RT/4F)\ln[P^3_{CO_2}(w)] + (RT/4F)\ln[P^2_{CO_2}(r)P_{O_2}(r)] \quad (4)$$

and E° is the anode potential at standard conditions, R is the universal gas constant, T is the cell temperature, $P_{CO_2}(w)$ is the CO_2 partial pressure at the working electrode, while $P_{CO_2}(r)$ and $P_{O_2}(r)$ are the partial pressures of CO_2 and O_2 at the reference electrode, respectively.

Various carbon fuels have been tested in different DCFC apparatus to investigate the efficacy of carbon fuels in the anodic reaction. It has been found that disordered carbon is more reactive due to the existence of more edge sites and defects, and graphitic carbon with high electrical conductivity may also benefit the electrochemical reaction. The physical and chemical properties of carbon fuels

* Corresponding author. Fax: +61 7 3365 4199.
E-mail address: z.zhu@uq.edu.au (Z. Zhu).

0378-7753/$ – see front matter © 2008 Elsevier B.V. All rights reserved.
doi:10.1016/j.jpowsour.2008.09.070

can thus influence their electrochemical performance. Weaver et al. [13] observed that carbon fuels with high surface area, such as devolatilized coal, are more accessible to the anode reaction, whereas Cooper's group [2,3] concluded that the effect of carbon surface area on discharge rate is not strong. Consequently, ways of improving the electrochemical reactivity of carbon fuels in the anode [i.e., reaction given by Eq. (1)] is still a major obstacle to the application of the DCFC.

Carbon materials are widely used in fuel cells as electrodes, electrocatalyst supports and hydrogen materials [20]. It is well known that the kinetics of the electrochemical processes involving carbon depend strongly on the surface characteristics of the carbons used. Surface treatments, including acid, heat, laser, plasma and electrochemical treatment, are usually applied to the carbon materials in order to enhance their electrochemical reactivity [21]. To our knowledge, no published study has been conducted on the relationship between the surface modification of carbon fuels and their electrochemical performances in a DCFC (rather than carbon electrodes). Thus, it was deemed appropriate to conduct a comparative investigation of the DCFC performance of two commercial carbon fuels including one activated carbon (AC) and one carbon black (CB) with different surface treatments employing HNO_3, HCl and plasma treatments. The electrochemical reactivities of these carbon fuels in the DCFC were systematically analysed, and correlated with physical and chemical characterization data on the surface chemistry and physics of the fuels.

2. Experimental

2.1. Preparation of carbon fuels

A commercial granular activated carbon (Calgon BPL, 0.25–0.45 mm particle size) and a carbon black sample (Koppers Continex N220, 0.1–0.2 mm particle size) were selected as the starting samples, which were designated as AC and CB, respectively. The acid treatment of AC and CB was by immersion in 4 M HNO_3 and 4 M HCl at room temperature for 24 h with subsequent washing with distilled water. These acid-treated carbon fuels are designated as AC-HNO_3, AC-HCl, CB-HNO_3 and CB-HCl, respectively. Air plasma treatment for the CB samples was carried out using a microwave generator (Sairem, France) with 2.45 GHz frequency and 100 W power. The reactor was first evacuated to a pressure of about 8000 Pa (60 Torr), then the CB was treated in air plasma for 15 min, which is designated as CB-Plasma.

2.2. Characterization of carbon fuels

X-ray diffraction (XRD) characterization of the carbon samples was performed with a Rigaku Miniflex X-ray diffractometer (40 kV, 30 mA) with Cu Kα radiation at a scanning rate of $2^\circ\ min^{-1}$ in the 2θ range from 10° to 90°. The average size of the carbon crystallites was calculated from the Debye–Scherrer equation:

$$L = \frac{K\lambda}{\beta\ \cos\theta} \quad (5)$$

where λ is the wavelength of the X-rays, θ is the diffraction angle, K is the shape factor, and β is the peak width at half-maximum intensity. Values of $K = 0.89$ and 1.84 [22,35] were used for L_c and L_a, respectively. The crystallite size perpendicular to the basal plane, L_c, was obtained from the (0 0 2) reflection, while the crystallite size parallel to the basal plane, L_a, was calculated using the (1 0 0) reflection corresponding to the a-axis unit cell parameter.

Electrical conductivities were measured by a frequency response analyser (Solartron SI1260). Approximately 200 mg of carbon material was pressed into a small pellet (13 mm diameter) at the lowest pressure needed to form a compact, namely, 150 kg cm^{-2}. The sample pellet was then placed between two gold-plated blocking electrodes of area 0.5 cm^2 in a jig of known resistance and the sample impedance was measured over the frequency range 1 MHz to 1 Hz using a sinusoidal excitation amplitude of 10 mV root mean square (rms). Finally, the bulk conductivity σ (S cm^{-1}), was calculated from:

$$\sigma = l[(r - r_0)A] \quad (6)$$

where l is the sample pellet thickness (cm), r is the tested sample resistance (Ω) taken as the impedance at zero phase angle, r_0 is the rig short-circuit resistance (Ω), and A is the electrode contact area (0.5 cm^2).

Nitrogen adsorption/desorption experiments were performed with a Quadrasorb adsorption analyser (Quantachrome, USA) at −196 °C. The specific surface area (S_{BET}) of each carbon samples was calculated by the multiple point Brunauer–Emmett–Teller (BET) method in the relative pressure range $P/P_o = 0.05$–0.25. The total pore volume (V_{total}) was derived from the adsorption amount at a relative pressure of $P/P_o = 0.99$. The average pore diameters (D_{pore}) of carbons were calculated by the available software (QuadraWin V2.0), which applies the Barrett–Joyner–Hallenda (BJH) method. The micropore volume (V_{micro}) and surface area (S_{micro}) of samples were also calculated by the available software (QuadraWin V2.0), which applies the Dubinin–Radushkevich (DR) method. Prior to the N_2 adsorption measurements, all samples were degassed overnight at 200 °C.

Temperature-programmed oxidation (TPO) measurements were conducted under air-flow (80 ml min^{-1}) in a thermogravimetric analyser (Shimadzu TGA-50). Samples were loaded into a platinum pan and heated under a nitrogen atmosphere from room temperature to 200 °C, and held for 1 h to remove the adsorption water, and then the temperature was further increased to 900 °C in air (80 ml min^{-1}) with a heating rate of 10 °C min^{-1}.

X-ray photoelectron spectroscopy (XPS) measurements were conducted using a Kratos Axis Ultra XPS system incorporating a 165 mm hemispherical electron energy analyser. The incident radiation was monochromatic Al Kα X-ray (1486.6 eV) at 150 W (15 kV, 10 ma). Survey scans were taken at an analyser pass energy of 160 eV, and performed over a 1200 eV binding energy range using a 1.0 eV step and a dwell time of 100 ms.

The mass titration method of Noh and Schwarz [31] was used to estimate the point of zero charge (PZC) of the carbon surfaces, at which the net total (external and internal) surface charge of the carbon particles is zero. This is based on the fact that the pH of the solution changes in the direction of the PZC on contact with the carbon particles [32]. Three different initial pH solutions (pH 3, 6, 11) were prepared using HNO_3 (0.1 M) and NaOH (0.1 M). Sodium nitrate was used as the background electrolyte. For each initial pH, six containers were filled with 20 ml of the solution and different amounts of carbon were added (0.05, 0.10, 0.50, 1.00 and 10% by weight). The equilibrium pH was measured after 24 h. The plot of pH versus mass fraction showed a plateau and the PZC is identified as the point at which the change in pH was negligible. The PZC was then taken as the average of the three asymptotic pH values.

Temperature-programmed desorption (TPD) experiments were carried out in a vertical tube furnace using Ar (80 ml min^{-1}) as the carrier gas. A 0.5 g sample was placed in a quartz tube, heated to 110 °C and held for 60 min and then ramped at 5 °C min^{-1} to 900 °C. The gases evolved were analysed using a gas chromatograph (Shimadzu GC-17A) equipped with a thermal conductivity detector and a Carbosphere column.

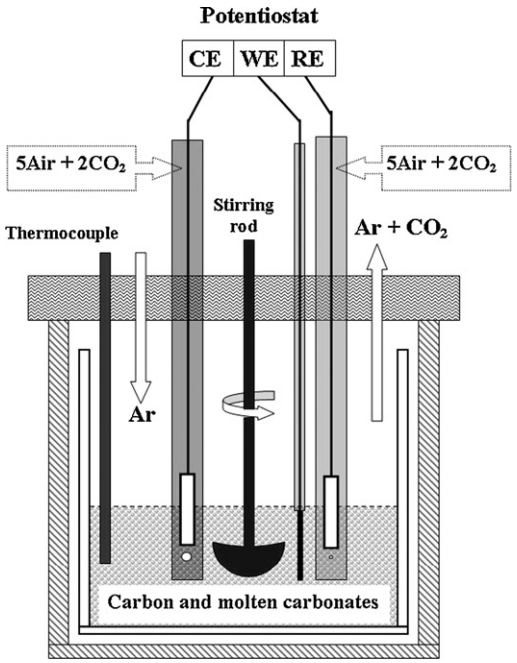

Fig. 1. Schematic diagram of direct carbon fuel cell.

2.3. Evaluation of carbon fuels in the DCFC

A schematic diagram of the DCFC is given in Fig. 1, which is similar to that of Vutetakis et al. [11,12]. The working electrode (WE) consisted typically of a solid gold rod (serving as the electrode and current collector, 99.9% purity, 3.2 mm diameter) cemented to the end of an alumina tube. A gold wire was spot-welded to the gold rod and extended to the other end of the alumina tube for external contact. The total exposed surface of the gold rod was 3.0 cm^2. The counter electrode (CE) was made from a gold sheet (with 1.0 cm^2 surface area) spot-welded to a gold wire, and the gold parts were sheathed in a 12 mm diameter closed-bottom alumina tube. A 1.5 mm hole at the bottom of the alumina sheath allowed contact through the electrolyte between the CE and WE. The reference electrode (RE) was constructed from an alumina sheath (12 mm diameter) containing a gold wire in contact with the electrolyte melt, and a 0.1 mm pin hole at the bottom of the alumina sheath provided contact of the electrolyte between the RE and WE. The particulate carbon fuels with the ternary molten carbonate electrolytes (32% Li–34% Na–34% K eutectic) were contained in an alumina crucible. In order to keep the entire cell in a gas-tight environment, the alumina crucible was placed at the bottom of an inconel canister and sealed by a water-cooled brass lid. The three electrodes and gas feed tubes were supported by the brass lid and inserted into the WE anode compartment. An inconel stirring rod with a half-circle impeller and a type-K thermocouple were also placed in the molten carbonate electrolyte.

Prior to each experiment, the dried 250 g ternary carbonate powder was mixed to a certain concentration (typically 1, 5 and 10% by weight) of carbon fuel powder. The gold parts of three different electrodes were washed by aqua regia for 10 s and rinsed with distilled water followed by acetone. After the fuel cell was assembled and sealed gastight, it was heated by a crucible furnace (Lindberg Blue/M) at a heating rate of 3 °C min^{-1}. During the heat-up stage, the Ar (150 ml min^{-1}) was purged into the WE compartment and CO_2 (50 ml min^{-1}) was purged into the CE and RE compartments. Once the required operating temperature was reached, the Ar and CO_2 purge rates were decreased to 50 and 14 ml min^{-1}, respectively.

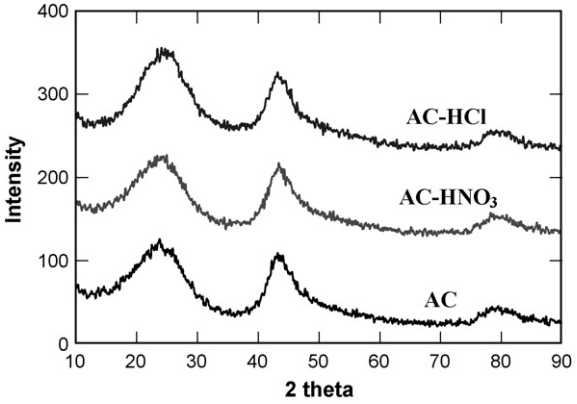

Fig. 2. X-ray diffraction patterns of AC, AC-HNO_3 and AC-HCl.

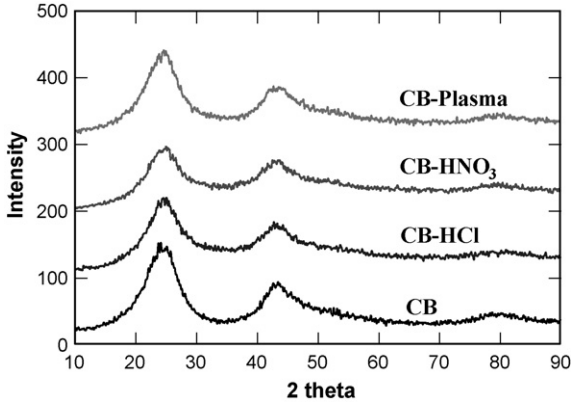

Fig. 3. X-ray diffraction patterns of CB, CB-HNO_3, CB-HCl and CB-Plasma.

At the same time, air (35 ml min^{-1}) was introduced into the CE and RE compartments. Finally, carbon anode half-cell measurements were performed with a potentiostat (Autolab PGSTAT302), using the GPES and FRA software package (Version 4.9). For the linear sweep voltammetry measurements, the anode was swept from the open circuit voltage (OCV) to 0.0 V (relative to the RE) at a scan rate of 1 mV s^{-1}. Note that under open-circuit conditions, the potential of the reference electrode is the same as the cathode and therefore the potential difference between the anode and reference is taken as the OCV. For on-line measurements of anodic product gases (evolved from the WE), the gas flow rate was measured by a soap film burette, and the gas compositions were analysed by a gas chromatograph (SHIMADZU GC-8A) with H_2 as the carrier gas.

3. Results

3.1. XRD characterizations of carbon fuels

Figs. 2 and 3 show the XRD patterns of AC and CB before and after surface treatments (HNO_3, HCl and air plasma). Only slight changes occur in the patterns for both AC and CB after various treatments. The asymmetrical (0 0 2) peak can be observed at around $2\theta = 24°$ for all carbon fuels. Another weak and broad peak at around $2\theta = 44°$ is attributed to the (1 0 0) graphite crystal face reflection.

The quantitative crystallite parameters of all carbon fuels are summarized in Table 1 including interplanar spacings (d_{002}), the average crystallite diameter (L_a) and the average crystallite stacking height (L_c). Acid treatments with HNO_3 or HCl led to an increase

Table 1
Crystalline parameters and electrical conductivities of carbon fuels.

Carbon fuel samples	XRD			Electrical conductivity σ (S cm^{-1})
	d_{002} (nm)	L_c (nm)	L_a (nm)	
AC	0.373 (5)	1.0 (1)	4.5 (3)	0.82 (5)
AC-HNO_3	0.353 (4)	1.2 (1)	4.8 (3)	0.88 (6)
AC-HCl	0.356 (4)	1.1 (1)	4.6 (3)	0.83 (5)
CB	0.368 (5)	1.5 (1)	2.9 (2)	1.54 (12)
CB-HNO_3	0.356 (4)	1.7 (2)	3.8 (3)	1.69 (13)
CB-HCl	0.363 (5)	1.6 (2)	3.7 (3)	1.59 (12)
CB-Plasma	0.361 (5)	1.5 (2)	4.6 (4)	1.72 (14)

in both L_a and L_c crystallite size parameters and decreases in the d_{002} values corresponding to decreases in the lattice parameter along the *c*-axis of the unit cell. By contrast, HNO_3 seems to be more effective in increasing the crystallite sizes in the carbon fuels compared to HCl. These results confirm that an acid treatment can increase the carbon aggregation and degree of graphitic structure to a certain extent [23]. Interestingly, air plasma treatment has the most significant effect on the carbon crystallite structure as shown in the last row of Table 1. The observed L_a value of CB-Plasma increases from 2.9 to 4.6 nm with the d_{002} decreasing from 0.368 to 0.361 nm, which may be caused by burning off of disordered carbon in CB during air plasma treatment [24,25].

3.2. Electrical conductivity of carbon fuels

Electrical conductivity of the carbon fuel is a critical factor governing DCFC performance, since carbon fuels will not only be consumed in the electrochemical reaction, but also be contacted with the current collector to transfer directly the electrons [2]. The electrical conductivity is highly dependent on the degree of graphitic structure of the fuel carbons. Usually, a higher degree of graphitic structure leads to a higher electrical conductivity. The bulk conductivity values of the two groups of carbon fuels are listed in column 5 of Table 1. After acid and air plasma treatments, the conductivities of AC and CB are improved slightly. In particular, CB-Plasma shows the highest conductivity (1.72 S cm^{-1}) for all carbon fuels, which is correlated with the fact that it has the highest degree of graphitic structure. Surprisingly, the AC series has a much lower conductivity than the CB series. This is probably caused by the air existing in highly porous AC series samples (even though the carbons were pressed into small pellets under pressure) and the air increased the electrical resistance in the conductivity tests.

3.3. Textural properties of carbon fuels

The nitrogen adsorption isotherms of AC, AC-HNO_3 and AC-HCl are shown in Fig. 4. These AC samples present typical type-I isotherms that are indicative of highly microporous structures. The appearance of hysteresis loops in the isotherms implies the existence of a mesoporous structure. The BET surface areas and pore structures of the three AC samples are presented in Table 2. Compared with untreated AC, the surface area and pore volume of AC-HNO_3 and AC-HCl have hardly changed, as shown in the rows 1–3 of Table 2. It has been reported that HNO_3 treatment may show a stronger effect on the textural changes of AC than HCl treatment due to the fixation of surface oxygen complexes at the entrance of micropores, or the collapse of some pore walls by HNO_3 treatment [26,27]. This is not obvious in our study since HNO_3 has a larger effect on the pore structure of AC but less effect on that of CB as shown in Table 2.

Fig. 5 compares the N_2 adsorption isotherms of CB samples before and after different treatments. All of the CB samples principally showed the type-IV characteristic, with a hysteresis loop that starts from medium relative pressures and closes at $(P/P_0) \approx 1$. The derived values of BET surface area, total pore volume and average pore diameter of these CB samples are summarized in rows 4–7 of Table 2. Increases in specific surface area and pore volume can be clearly observed when CB is treated with acid and air plasma, which is probably attributed to the removal of ash or organics in the CB particles [25,28].

3.4. Chemical reactivity of carbon fuels in TGA

Fig. 6 shows the weight loss curves of AC, AC-HNO_3 and AC-HCl in air obtained by TGA tests. For all three samples, a small weight loss can be observed below 100 °C due to the desorption of water. The oxidation of carbonaceous species is observed over the

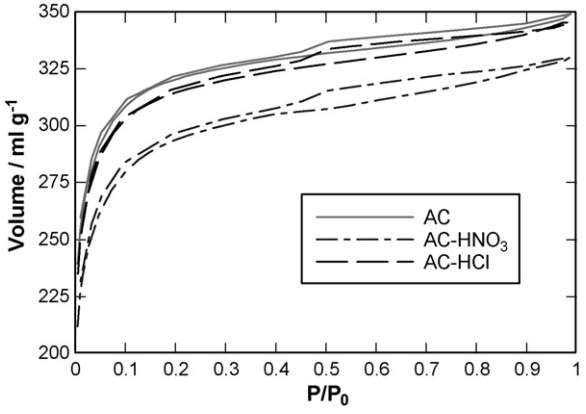

Fig. 4. Nitrogen adsorption isotherms of AC, AC-HNO3 and AC-HCl.

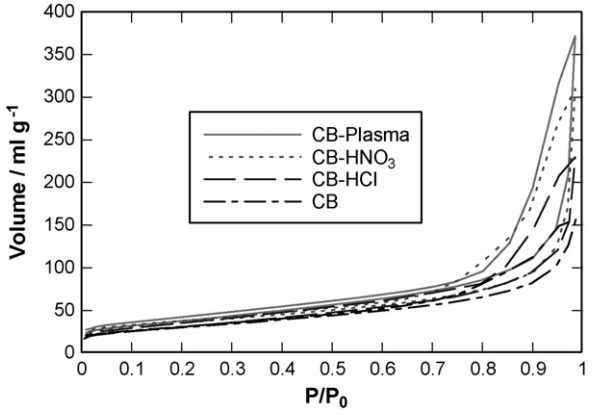

Fig. 5. Nitrogen adsorption isotherms of CB, CB-HNO_3, CB-HCl and CB-Plasma.

Table 2
Textural properties of carbon fuels.

Carbon samples	N_2 adsorption				
	S_{BET} ($m^2\ g^{-1}$)	V_{total} ($cm^3\ g^{-1}$)	D_{pore} (nm)	S_{micro} ($m^2\ g^{-1}$)	V_{micro} ($cm^3\ g^{-1}$)
AC	1225 (123)	0.538 (27)	0.88 (4)	1193 (119)	0.491 (25)
AC-HNO_3	1082 (108)	0.514 (26)	0.91 (5)	1018 (102)	0.427 (21)
AC-HCl	1204 (120)	0.532 (26)	0.89 (4)	1157 (116)	0.473 (24)
CB	107 (10)	0.243 (12)	4.56 (24)	9 (1)	0.004 (1)
CB-HNO_3	125 (12)	0.482 (24)	7.61 (38)	16 (2)	0.008 (1)
CB-HCl	113 (11)	0.351 (17)	5.97 (30)	7 (1)	0.003 (1)
CB-Plasma	136 (13)	0.567 (28)	8.52 (43)	6 (1)	0.003 (1)

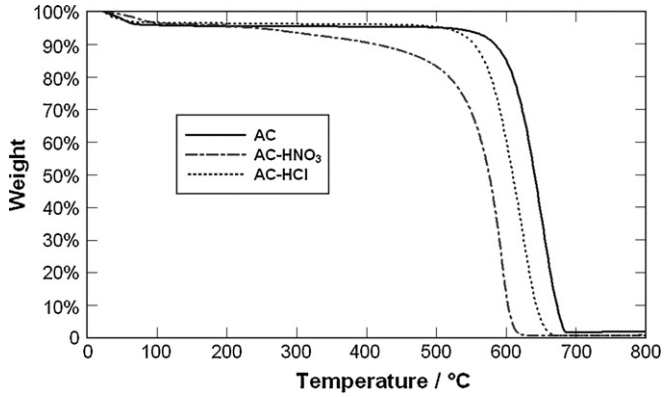

Fig. 6. Thermogravimetric analyser curves of AC, AC-HNO_3 and AC-HCl.

range of 450–700 °C. For AC-HNO_3, there is another small weight loss below 450 °C due to the decomposition of surface functional groups. It is known that the presence of a large amount of surface oxygen functional groups may lead to carbon materials that are highly reactive, thereby decreasing the thermal stability of AC-HNO_3 in TPO tests [27,29]. For AC-HCl, the onset of oxidation starts around 550 °C, which is slightly lower than that of AC (600 °C). The thermal stability of three carbon fuels decrease in the order AC > AC-HCl > AC-HNO_3.

The weight losses of the CB series before and after various treatments are given in Fig. 7. Compared with AC, the weight loss of physisorbed water below 100 °C for CB is much less. The onset of oxidation of the as-received CB is observed from 550 °C. Similar to the acid treatment of AC samples, CB-HNO_3 and CB-HCl are more readily oxidized than untreated CB. For CB-HNO_3, the extensive weight loss starts from 500 °C and ends at around 600 °C, which correlates with the burn-off of carbonaceous species. Below 500 °C, there is another small weight loss of CB-HNO_3 owing to the decomposition of surface functional groups. For CB-HCl, the onset of oxidation lies around 550 °C, which is slightly lower than that of original CB. CB-Plasma had the best oxidation resistance in all carbon black samples, which may be due to it having the highest graphitic degree as shown in Table 1.

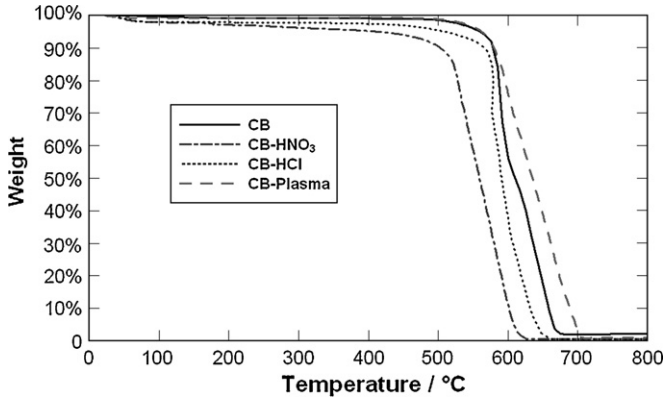

Fig. 7. Thermogravimetric analyser curves of CB, CB-HNO_3, CB-HCl and CB-Plasma.

3.5. Surface properties of carbon fuels

The atomic concentrations of carbon and oxygen on the carbon fuels surface obtained by survey scans in XPS are listed in Table 3. The ratio of total O to C (O:C) is indicative of the degree of surface oxidation of carbon fuel. In general, all treated carbon fuels show an increase in the surface oxygen content as expected. The HNO_3-treated carbon fuels (AC-HNO_3 and CB-HNO_3) show the highest oxygen content in all of the carbon samples. Furthermore, the AC series present higher surface oxygen contents than the CB series under the same treatment probably owing to the different microstructures and textual properties.

In order to confirm further the extent of oxidation of different carbon fuels, the PZC values of all carbon fuels (determined by mass titration method) are given in the last column of Table 3. The as-received AC and CB carbons showed PZC values of 10.04 and 8.23, respectively. These PZC values diminish after a variety of treatments. Especially, the samples treated with HNO_3 have the lowest PZC values, in agreement with previous reports [30] that HNO_3 treatment could increase the amounts of the acidic carboxyl and lactone surface groups. The PZC of CB-Plasma is only slightly lower than CB, however, and this indicates that the air plasma treatment does not change the surface properties of CB substantially. It is known that more oxidized carbon usually has the lower PZC value [31]. The order of the amount of oxygen on the surface of the AC series is AC-HNO_3 > AC-HCl > AC. For the CB series, the oxygen amount on the surface is of the order CB-HNO_3 > CB-HCl > CB-Plasma > CB.

The CO_2 and CO evolution profiles with increasing temperature from the surfaces of three activated carbon fuels are given in Fig. 8. As expected, AC with HNO_3 treatment generates intense oxygen functional groups on the carbon that leads to the production of the largest amounts of CO_2 and CO in the Ar gas stream. By contrast, the samples AC-HCl and AC have comparably lower evolution

Table 3
X-ray photoelectron spectroscopy and mass titration analyses of surface properties of carbon fuels.

Samples	O (%)	C (%)	O:C	PZC
AC	8.0	90.8	0.088	10.04
AC-HNO_3	10.6	88.1	0.121	3.15
AC-HCl	9.1	90.1	0.101	7.34
CB	1.9	97.9	0.019	8.23
CB-HNO_3	9.3	88.9	0.105	3.35
CB-HCl	5.5	93.3	0.058	4.42
CB-Plasma	2.6	97.0	0.026	8.16

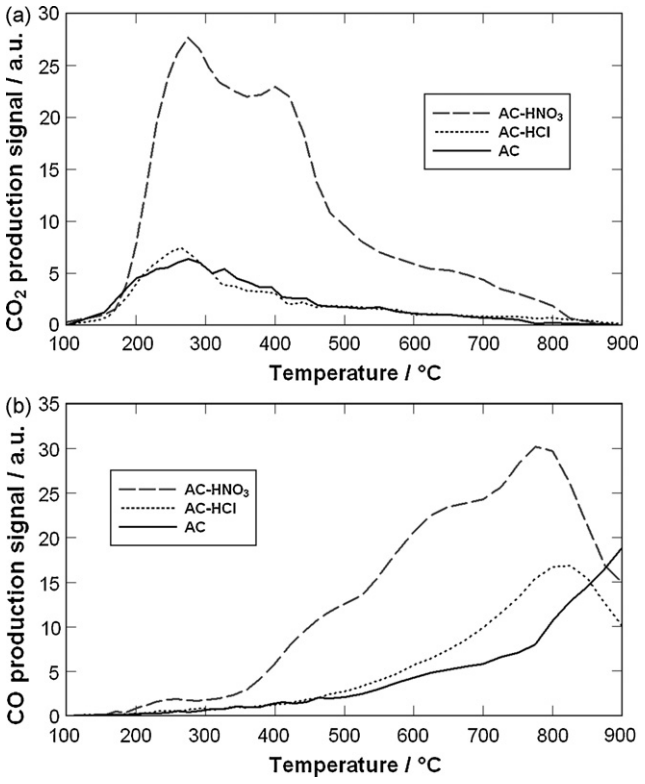

Fig. 8. Temperature-programmed desorption profiles of (a) CO_2 and (b) CO from AC-HNO_3, AC-HCl and AC.

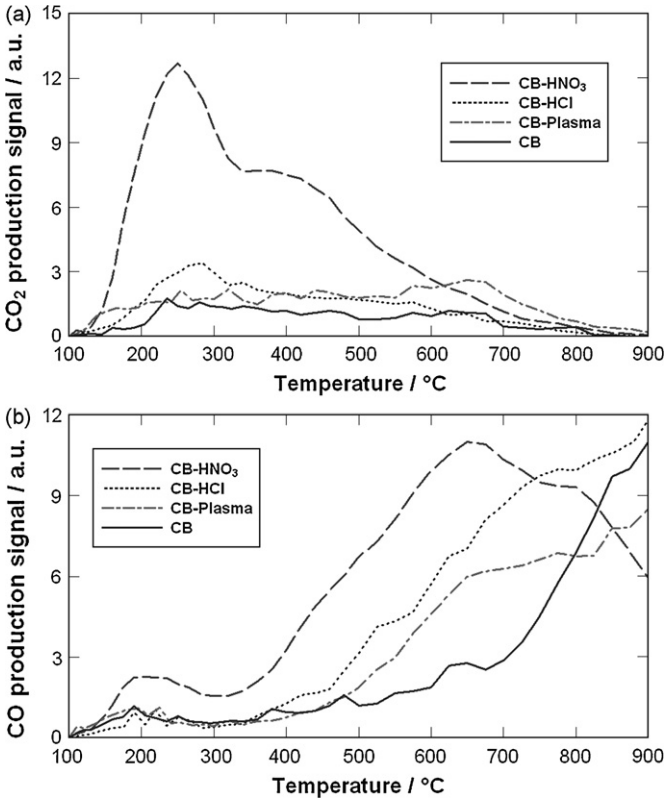

Fig. 9. Temperature-programmed desorption profiles of (a) CO_2 and (b) CO from CB-HNO_3, CB-HCl, CB-Plasma and CB.

of CO_2 and CO complexes, and different thermal stabilities. In the CO_2 evolution spectra, the AC-HNO_3 presents double peaks around 275 and 400 °C. AC-HCl and AC have a single broad peak in the range 200–400 °C, but AC-HCl shows a maximum around 270 °C. These results indicate that the AC-HNO_3 has a larger number of carboxyl and lactone surface functional groups than the other two carbon samples, in agreement with the results of PZC and XPS. From the CO evolution curves, the two acid-treated AC samples seem to have more active CO complexes than untreated AC, since AC-HNO_3 and AC-HCl present peaks at 770 and 820 °C, respectively, while the desorbed CO concentration on AC is still increasing at 900 °C.

The TPD profiles of CB before and after the different surface treatments are presented in Fig. 9. Compared with original CB, the treated CB samples present an increase in the amount of surface oxygen functional groups, which is evidenced by the increase of the CO_2 and CO peak heights and areas. Especially for CB-HNO_3, the evolution of CO_2 shows the sharpest peak at 250 °C and a shoulder at around 425 °C, with CO desorption peaks at 700 °C. By comparison, the CB-HCl and CB-Plasma samples have much lower evolution of CO_2 than CB-HNO_3. CB-Plasma has more stable CO_2-yielding surface complexes than CB-HCl. From the CO evolution spectra, CB-Plasma shows slightly lower evolution than CB-HCl from 400 to 900 °C. This further confirms that the CB-Plasma has less total surface oxygen functional groups compared with CB-HCl and CB-HNO_3.

In general, HNO_3 treatment results in large amounts of CO_2-yielding functional groups on the surface of AC and CB. On the other hand, HCl treatment lowers the stability of CO-yielding surface groups on the carbon surface, which can thus be desorbed at a lower temperature in the TPD tests. Air plasma treatment has a similar effect on the carbon surface as that of HCl treatment.

3.6. Electrochemical reactivity of carbon fuels in DCFC

Fig. 10 presents the anodic polarization curves of 5% AC, AC-HNO_3 and AC-HCl at 700 °C with 600 rpm stirring condition. The polarization curves of the three AC carbon fuels are similar in shape. The curves all fall steeply from the OCVs to around −0.8 V due to the activation resistance. Following that, a more stable linear region appears from −0.8 to −0.4 V, which indicates that the potential at the anode is under significant ohmic resistance control. Finally, the potential decreases sharply at high current density as fuel is consumed faster than it is supplied to the electrode, which is known as a mass transport-limitation. In these three carbon fuels, the AC-HNO_3 displays the highest electrochemical reactivity, since it has the highest current density at a given potential. Although AC and AC-HCl have comparably low electrochemical reactivities in the

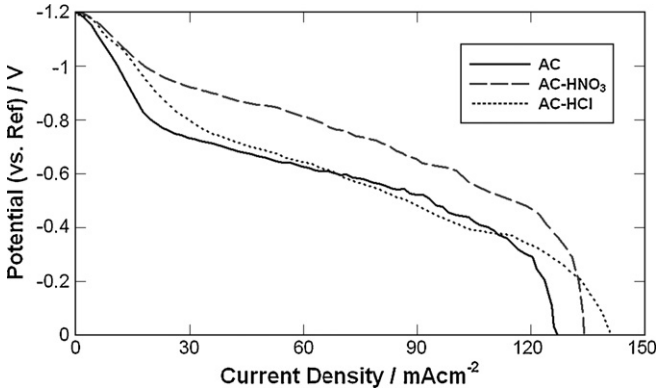

Fig. 10. Polarization curves and of 5 wt.% AC series carbon fuels at 700 °C with 600 rpm stirring.

Table 4
Electrochemical data of AC, AC-HNO_3 and AC-HCl at different temperature.

Conditions		AC	AC-HNO_3	AC-HCl
600 °C 600 rpm	OCV (V)	−1.02	−1.05	−1.03
	I at −0.9 V (mA cm^{-2})	7.7	13	9.3
	I at −0.6 V (mA cm^{-2})	19	40	22
	I at −0.3 V (mA cm^{-2})	34	55	43
	Rs (Ω cm^{-2})	22.7	10.2	14.3
700 °C 600 rpm	OCV (V)	−1.2	−1.21	−1.19
	I at −0.9 V (mA cm^{-2})	14.8	35.6	21
	I at −0.6 V (mA cm^{-2})	69	100	68
	I at −0.3 V (mA cm^{-2})	118	130	124
	Rs (Ω cm^{-2})	4.3	4.0	5.5
800 °C 600 rpm	OCV (V)	−1.34	−1.35	−1.33
	I at −0.9 V (mA cm^{-2})	36.5	86	53.5
	I at −0.6 V (mA cm^{-2})	118	160	132
	I at −0.3 V (mA cm^{-2})	240	260	208
	Rs (Ω cm^{-2})	2.9	2.6	3.8

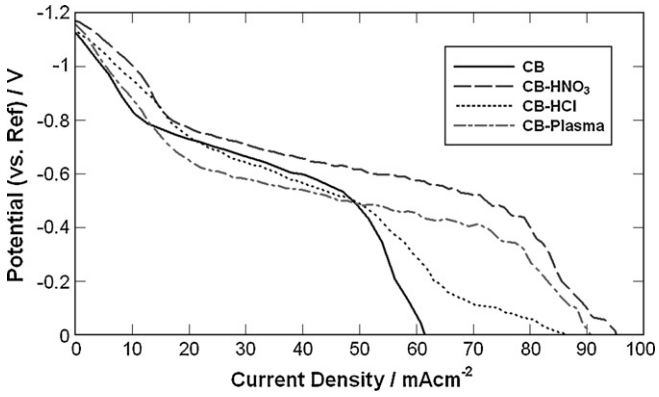

Fig. 11. Polarization curves of 5 wt.% CB series carbon fuels at 700 °C with 600 rpm stirring.

DCFC, the latter shows a higher current density than the former in the low over-potential region (from OCV to −0.8 V). It is known that the current densities in this region are dominated by the rates of the relevant electrochemical reactions. These results indicate that acid treatments (HNO_3 and HCl) of AC can effectively improve the electrochemical reaction rates.

Table 4 provides a detailed comparison of the OCV and current density (I) at given potentials and specific area resistance (Rs) of AC, AC-HNO_3 and AC-HCl. The OCV values of the three carbon fuels are similar at the same temperature, and they all become more negative when the temperature increases from 600 to 800 °C. This change in the OCV is caused by the shift of anodic electrochemical equilibrium as discussed by other researchers [7,9–12,17]. Under the same experimental conditions, AC-HNO_3 always gives the highest current density of the three carbon fuels, which means that AC-HNO_3 has a faster discharge rate than the other carbons. AC-HCl and AC show comparably lower current densities (especially from the medium-to-higher overpotential regions). Rs is the slope of the anodic voltage versus the current density in the linear central region of polarization curve [14], and is a measurement for the global ohmic resistance which arises from the carbon fuels and electrolytes, the electrode materials, and even the mechanical connections within the cell apparatus. The Rs values at 600 °C are much higher than those at 700 and 800 °C since the electrical conductivity of molten carbonate increases significantly with increasing temperature [11,12,19]. At the same temperature, AC-HNO_3 has the lowest Rs value in three carbon samples and this correlates with it having the highest electrical conductivity, as shown in Table 1. On the whole, the electrochemical reactivities of the three AC carbon fuels are in the order AC < AC-HCl < AC-HNO_3.

Fig. 11 presents the anodic polarization curves of the four CB carbon fuels at 700 °C with 600 rpm stirring conditions. Similarly, these carbon fuels all display typical three-phase regime polarization curves to the AC carbon fuels, which can be attributed to the activation, ohmic and concentration overpotential regimes, respectively. The CB-HNO_3 shows the highest current density or the highest electrochemical reactivity. Although the CB, CB-HCl and CB-Plasma have similar low values in the ohmic region, the treated CB fuels (CB-HCl and CB-Plasma) show higher current densities than the untreated CB in both the activation and concentration regions. This indicates that acid and plasma treatments can improve the CB electrochemical reaction rate to different extents.

Table 5 provides a comparison of OCV, current density (I) at given potentials, specific area resistance (Rs) of the CB series of carbon fuels. Compared with the AC series, these four CB carbon fuels have much lower current densities at the same given potentials and thereby indicate that the CB series are less active in the DCFC reaction. On the other hand, the discharge rate of CB can effectively be increased by acid and air plasma treatments, which is similar to the AC carbon fuels. Especially with the HNO_3 treatment, the current density of CB-HNO_3 is 2–3 times higher than that of original CB. This is consistent with altered microstructure and surface properties of CB-HNO_3, which will be addressed in detail in Section 4. The HCl and air plasma pre-treated CB have a lower electrochemical reactivity than CB-HNO_3. Interestingly, the CB-Plasma shows the lowest Rs value that may be caused by it having the highest electrical conductivity of all the carbon samples (see Table 1). In general, the electrochemical reactivities of the four CB carbon fuels increase in the order: CB < CB-HCl ≈ CB-Plasma < CB-HNO_3.

3.7. Anodic off-gas analysis

In order to study the electrochemical kinetics at the anode, Table 6 compares the gas evolution data from the WE compartment using 5 wt.% AC, AC-HNO_3 and AC-HCl at 600, 700 and 800 °C

Table 5
Electrochemical data of CB, CB-HNO_3, CB-HCl and CB-Plasma at 700–800 °C.

Conditions		CB	CB-HNO_3	CB-HCl	CB-Plasma
700 °C 600 rpm	OCV (V)	−1.13	−1.17	−1.14	−1.16
	I at −0.9 V (mA cm^{-2})	7	13	11	9
	I at −0.6 V (mA cm^{-2})	38	54	35	23
	I at −0.3 V (mA cm^{-2})	55	83	59	78
	Rs (Ω cm^{-2})	8.3	6.5	8.5	5.6
800 °C 600 rpm	OCV (V)	−1.26	−1.31	−1.28	−1.29
	I at −0.9 V (mA cm^{-2})	16	46	32	22
	I at −0.6 V (mA cm^{-2})	47	67	50	49
	I at −0.3 V (mA cm^{-2})	80	93	78	77
	Rs (Ω cm^{-2})	7.5	5.8	7.2	4.9

Table 6
Anodic off-gas data of 5 wt.% AC, AC-HNO_3 and AC-HCl at 600–800 °C with 600 rpm.

		X_{Ar} (%)	X_{CO} (%)	X_{CO_2} (%)	Q_{Total} (ml s^{-1})	Q_{CO_2} (ml s^{-1})	Y_{CO_2}	$Q_{(CO_2+CO)}$ (ml s^{-1})	$Y_{(CO_2+CO)}$
AC									
600 °C	I-off	97.2	0.3	2.1	1.34 (2)	0.015 (2)	0.59 (5)	0.017 (2)	0.65 (6)
	I = 0.10 A	96.4	0.4	3.1	1.42 (2)				
700 °C	I-off	90.6	5.3	3.8	1.38 (2)	0.032 (3)	0.63 (6)	0.036 (3)	0.70 (7)
	I = 0.20 A	88.9	5.2	5.7	1.47 (2)				
800 °C	I-off	89.9	9.0	0.9	1.41 (2)	0.014 (2)	0.28 (2)	0.053 (5)	1.03 (10)
	I = 0.20 A	87.0	11.1	1.8	1.50 (3)				
AC-HNO_3									
600 °C	I-off	96.9	0.4	2.5	1.36 (2)	0.018 (2)	0.71 (6)	0.019 (2)	0.73 (7)
	I = 0.10 A	95.7	0.4	3.6	1.45 (2)				
700 °C	I-off	91.0	4.7	3.9	1.38 (2)	0.038 (4)	0.75 (7)	0.041 (4)	0.79 (8)
	I = 0.20 A	89.1	4.5	6.2	1.49 (2)				
800 °C	I-off	88.9	9.8	1.1	1.44 (2)	0.024 (2)	0.46 (5)	0.049 (5)	0.96 (10)
	I = 0.20 A	86.6	10.6	2.5	1.56 (2)				
AC-HCl									
600 °C	I-off	97.0	0.4	2.2	1.36 (2)	0.016 (2)	0.63 (6)	0.018 (2)	0.65 (7)
	I = 0.10 A	95.9	0.3	3.3	1.43 (2)				
700 °C	I-off	91.0	4.8	3.9	1.37 (2)	0.034 (3)	0.66 (6)	0.042 (4)	0.80 (8)
	I = 0.20 A	88.9	5.0	5.9	1.47 (2)				
800 °C	I-off	89.4	9.2	1.3	1.39 (2)	0.015 (2)	0.30 (3)	0.050 (5)	0.95 (10)
	I = 0.20 A	86.9	10.8	2.2	1.49 (2)				

X_{Ar}, X_{CO} and X_{CO_2}: concentration of Ar, CO and CO_2 in anodic off-gas by GC analysis. Q_{Total}: total anodic off-gas evolution rate by bubble-meter measurement. Q_{CO_2}: net electrochemical CO_2 evolution rate are calculated by Eq. (8). Y_{CO_2}: electrochemical CO_2 yield are calculated by Eq. (9). $Q_{(CO_2+CO)}$: net electrochemical CO_2 and CO evolution rate are calculated by Eq. (10). $Y_{(CO_2+CO)}$: electrochemical CO_2 and CO yield are calculated by Eq. (11).

with 600 rpm stirring. In the second column of Table 6, the off-gas composition was analysed by gas chromatography (GC) with the current off to give a baseline, and then with the current on to measure the gases produced by the electrochemical reaction. Only purge gas Ar and carbon oxides (CO and CO_2) are found at measurable levels in the GC analysis. The CO concentration increases with rising cell temperature but the CO_2 concentration increases slightly from 600 to 700 °C, and decreases sharply at 800 °C. This phenomenon may be caused by the following Boudouard reaction that can easily occur at temperatures above 750 °C [9,12,33]:

$$CO_2(g) + C(s) = 2CO(g) \quad (7)$$

The net electrochemical CO_2 evolution rate (Q_{CO_2}) can be calculated by the difference between the outlet CO_2 flow rate with current on and the CO_2 flow rate with current off [12], i.e.,

$$Q_{CO_2} = (X_{CO_2} Q_{Total})_{I-on} - (X_{CO_2} Q_{Total})_{I-off} \quad (8)$$

Consequently, the electrochemical CO_2 yield (Y_{CO_2}) can be calculated by [12]:

$$Y_{CO_2} = \frac{Q_{CO_2} F}{V_m I} \quad (9)$$

where F is the Faraday constant (96485 C mol^{-1}), V_m is the molar volume of CO_2 at 300 K and 1 atm (ml mol^{-1}) and I is the current applied in the gas measurements (A). Similarly, the total electrochemical product gas evolution rate ($Q_{(CO_2+CO)}$) and gas yield ($Y_{(CO_2+CO)}$) can be calculated as follows [12]:

$$Q_{(CO_2+CO)} = [(X_{CO_2} + X_{CO}) Q_{Total}]_{I-on} - [(X_{CO_2} + X_{CO}) Q_{Total}]_{I-off} \quad (10)$$

$$Y_{(CO_2+CO)} = \frac{Q_{(CO_2+CO)} F}{V_m I} \quad (11)$$

As shown in Table 6, Y_{CO_2} is around 0.6–0.75, and $Y_{(CO_2+CO)}$ ranges between 0.65 and 0.8 for the three AC samples at 600 and 700 °C, in agreement with the theoretical CO_2 yield of 0.75 in the assumed main anodic reaction as shown in Eq. (1). This indicates that the main product of the electrochemical oxidation of carbon at 600–700 °C is CO_2 rather than CO, consistent with previous reports [11,12]. However, the Y_{CO_2} decreases to 0.28–0.46 and $Y_{(CO_2+CO)}$ increases to 0.95–1.03 when the temperature rises to 800 °C. This may be caused by the Boudouard reaction, which consumes the formed CO_2 and carbon fuels at higher temperature. Alternatively, the electrochemical oxidation of carbon at 800 °C may be explained by [33,34]:

$$C(s) + CO_3^{2-} = CO_2(g) + CO(g) + 2e^- \quad (12)$$

where the theoretical value of the total gas evolution (CO_2 and CO) is 1.0. Under the same operational conditions, the AC-HNO_3 presents the highest Q_{CO_2} and Y_{CO_2} values in these three carbon fuels which means more AC-HNO_3 fuels participate in the electrochemical oxidation in the DCFC due to their highest reactivities.

The carbon efficiency (E_{Carbon}) is shown in Fig. 12. This evaluates the ratio of electrochemical oxidation of carbon via Eq. (1) to the total carbon consumption (chemical and electrochemical) and is calculated by [12]:

$$E_{Carbon} = \frac{(1/3)Q_{CO_2}}{(1/2)(X_{CO} Q_{Total})_{I-on} + (1/3)Q_{CO_2}} \times 100\% \quad (13)$$

where the coefficients are determined by the molar ratios of the gas products to one mole of reactant carbon consumed in Eqs. (1) and (7), respectively.

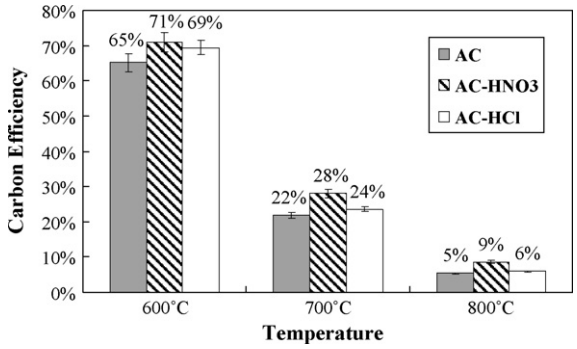

Fig. 12. Carbon efficiency of 5 wt.% AC, AC-HNO_3 and AC-HCl at 600–800 °C.

It can be seen that E_{Carbon} values decrease with increase in temperature, due to the parasitic chemical loss of carbon by the Boudouard reaction (7) at higher temperature. Especially at 800 °C, E_{Carbon} is less than 10%, which means more than 90% of carbon fuels are heavily consumed by the chemical rather than by the electrochemical reaction. Interestingly, at the same temperature, the treated carbon fuels (AC-HNO_3 and AC-HCl) present slightly higher carbon efficiencies than untreated AC, especially for AC-HNO_3. These results further confirm the improvement of electrochemical reactivity for acid-treated carbon fuels.

4. Discussion

Although the electrochemical oxidation of carbon fuels in the present investigation occurs in the heterogeneous carbon|carbonate and electrode|carbonate interfaces, the basic mechanism of carbon oxidation in molten carbonate is similar to the reactions of carbon with oxygen containing gases. It is well known that the carbon properties, such as degree of graphitic structure, surface area, pore structure, particle size and surface properties can influence the reaction of carbon gasification in oxygen. In the process of carbon oxidation, molecular oxygen dissociatively chemisorbs on to reactive carbon sites to form surface oxygen functional groups, and decomposes to form CO_2 and/or CO upon reaction. As a result of the removal of carbon atoms, new free reactive sites are exposed for subsequent chemisorption [35,36]. Therefore, the number of surface oxygen functional groups plays a key role in carbon gasification reactions.

In the present study, the improvement of electrochemical reactivity of treated AC and CB can be explained by dramatic changes in their surface properties after different treatments. In particular, the HNO_3-treated carbon fuels (AC-HNO_3 and CB-HNO_3) present much higher electrochemical reactivity than the other carbon fuels in the DCFC, which is mainly caused by the presence of high amounts of surface oxygen functional groups. As shown by the study of surface chemical properties (Section 3.5), the HNO_3-treated carbon fuels have the highest number of oxygen groups and this translates to a large number of free reactive sites. This is the major contribution to the enhanced anodic discharge rate in the DCFC tests. Meanwhile, the Rs of DCFC is decreased by using the HNO_3-treated carbon fuels and this feature may be attributed to an increase in their degree of graphitic structure. It may also be helpful for the performance of HNO_3-treated carbons, but its contribution may be limited. The carbon fuels treated with HCl or air plasma have lower electrochemical reactivities than the HNO_3-treated carbons. As mentioned above, the quantity of surface oxygen functional groups directly affects the electrochemical discharge rate of carbon fuels. With HCl or air plasma treatment, the carbons have markedly fewer surface oxygen functional groups than HNO_3-treated carbons, as shown in TPD and XPS studies. CB-Plasma has a lower Rs value than CB-HCl, which may be attributed to the highest degree of graphitic structure with CB-Plasma. Compared with AC carbons, CB carbons are much less reactive in the DCFC. This may be attributed primarily to the former's enhanced surface area, which provides more contact between the carbon fuels and the electrolytes.

5. Conclusions

Two groups of commercial carbon fuels (CB and AC) with different surface modifications have been evaluated in a DCFC system. Treatment with HNO_3 can dramatically improve the electrochemical reactivity of carbon fuels due to enhancement of the oxygen-containing surface functional groups that, in turn, may produce high amounts of active sites by desorption. Air plasma treatment has the greatest effect on the degree of graphitic structure of the carbon. The overall effect on changing the electrochemical reactivity of carbon fuels is of the order HNO_3 > air plasma ≈ HCl. The HNO_3-treated activated carbon, AC-HNO_3, gives the highest current density (240 mA cm^{-2} at −0.3 V). Complete oxidation of carbon to CO_2 can be achieved at 600–700 °C, while carbon is partially electrochemically oxidised to CO at 800 °C.

Acknowledgment

Financial Support from the Discovery Project of the Australian Research Council is greatly appreciated.

References

[1] D. Cao, Y. Sun, G. Wang, J. Power Sources 167 (2) (2007) 250–257.
[2] N.J. Cherepy, R. Krueger, K.J. Fiet, A.F. Jankowski, J.F. Cooper, J. Electrochem. Soc. 152 (1) (2005) A80–A87.
[3] J.F. Cooper, Proceedings of the Second International Conference on Fuel Cell Science Engineering and Technology, Rochester, NY, United States, June 14–16, 2004, pp. 375–385.
[4] J.F. Cooper, N. Cherepy, Carbon fuel particles used in direct carbon conversion fuel cells, US patent 845,939 (2004).
[5] J.F. Cooper, R. Krueger, N. Cherepy, A high temperature, molten electrolyte electrochemical cell comprising ash-free turbostratic carbon particles, US patent 970,283 (2001).
[6] K. Hemmes, M. S Cassir, Proceedings of the Second International Conference on Fuel Cell Science Engineering and Technology, Rochester, NY, United States, June 14–16, 2004, pp. 395–400.
[7] S. Zecevic, E.M. Patton, P. Parhami, Chem. Eng. Commun. 192 (10–12) (2005) 1655–1670.
[8] J. Dubois, J. Millet, S. Palous, Electrochim. Acta 12 (3) (1967) 241–244.
[9] V. Hauser, A study of carbon anode polarization in fused carbonate fuel cells. PhD thesis, Oregon State University, Corvallis, OR, USA, 1964.
[10] W.H.A. Peelen, M. Olivry, S.F. Au, J.D. Fehribach, K. Hemmes, J. Appl. Electrochem. 30 (12) (2000) 1389–1395.
[11] D.G. Vutetakis, Electrochemical oxidation of carbonaceous materials dispersed in molten carbonate, PhD thesis, Ohio State University, Columbus, OH, USA, 1985.
[12] D.G. Vutetakis, D.R. Skidmore, H.J. Byker, J. Electrochem. Soc. 134 (12) (1987) 3027–3035.
[13] R.D. Weaver, S.C. Leach, L. Nanis, Proceedings of the 16th Intersociety Energy Conversion Engineering Conference, vol. 1, 1981, pp. p717–721.
[14] G.A. Hackett, J.W. Zondlo, R. Svensson, J. Power Sources 168 (1) (2007) 111–118.
[15] T. Nunoura, K. Dowaki, C. Fushimi, S. Allen, E. Meszaros, M.J. Antal, Ind. Eng. Chem. Res. 46 (3) (2007) 734–744.
[16] P.V. Pesavento, Carbon-air fuel cell, US patent 6,200,697 (2001).
[17] S. Zecevic, E.M. Patton, P. Parhami, Carbon 42 (10) (2004) 1983–1993.
[18] T.M. Gur, R.A. Huggins, J. Electrochem. Soc. 140 (7) (1993) 1990–2000.
[19] K. Pointon, B. Lakeman, J. Irvine, J. Bradley, S. Jain, J. Power Sources 162 (2) (2006) 750–756.
[20] A.L. Dicks, J. Power Sources 156 (2) (2006) 128–141.
[21] K. Kinoshita, Carbon: Electrochemical and Physicochemical Properties, Wiley, New York, 1988.
[22] L. Li, Z.H. Zhu, G.Q. Lu, Z.F. Yan, R. De Marco, Appl. Catal. A: Gen. 309 (2) (2006) 201–209.
[23] S. Kim, S.J. Park, Electrochim. Acta 52 (9) (2007) 3013–3021.
[24] Z. Tang, Q. Li, G. Lu, Carbon 45 (1) (2007) 41–46.
[25] S.J. Park, J.S. Kim, J. Colloid Interface Sci. 244 (2) (2001) 336–341.
[26] J.L. Figueiredo, M.F.R. Pereira, M.M.A. Freitas, J.J.M. Orfao, Carbon 37 (9) (1999) 1379–1389.
[27] B.K. Pradhan, N.K. Sandle, Carbon 37 (8) (1999) 1323–1332.
[28] T. Takada, M. Nakahara, H. Kumagai, Y. Sanada, Carbon 34 (9) (1996) 1087–1091.
[29] P. Li, T.J. Zhao, J.H. Zhou, Z.J. Sui, Y.C. Dai, W.K. Yuan, Carbon 43 (13) (2005) 2701–2710.
[30] Z.H. Zhu, L.R. Radovic, G.Q. Lu, Carbon 38 (3) (2000) 451–464.
[31] J.S. Noh, J.A. Schwarz, Carbon 28 (5) (1990) 675–682.
[32] H.P. Boehm, Carbon 40 (2) (2002) 145–149.
[33] R.D. Weaver, S.C. Leach, A.E. Bayce, L. Nanis, Direct electrochemical generation of electricity from coal, Report for the period 16 May 1977–15 February, 1979, SRI, Menlo Park, CA 94025; SAN-0115/105-1.
[34] K. Sasaki, A. Kunai, T. Sada, Denki Kagaku 48 (5) (1980) 311–314.
[35] L.R. Radovic, P.L. Walker Jr., R.G. Jenkins, Fuel 62 (7) (1983) 849–856.
[36] A.A. Lizzio, H. Jiang, L.R. Radovic, Carbon 28 (1) (1990) 7–19.